

# *In Situ* Electrical Conductivity Measurement by Using Confocal Scanning Laser Microscopy



LING ZHANG, ANNELIES MALFLIET, BART BLANPAIN, and MUXING GUO

The mineralogy of a particular slag can be modified by steering the slag cooling process to valorise a particular slag in high added value applications. However, without online monitoring of the crystallization degree and temperature, it is challenging to control slag crystallization precisely. Since the electrical conductivity is sensitive to a minor change in the slag microstructure, electrical conductivity may be used to monitor the change in the composition of the liquid phase and the precipitation during slag solidification. In this work, an innovative experimental setup was developed using a confocal scanning laser microscope (CSLM) to measure the electrical conductivity of the slag while simultaneously observing slag solidification. Two types of high-temperature electrical conductivity cells are designed to determine the electrical conductivity of the slag. Each method's advantages and disadvantages are identified, and their potential applications are recommended. The techniques have been confirmed to be accurate and reliable for the electrical conductivity measurement of slag during the *in situ* observation of slag solidification, providing a powerful tool for slag valorization.

<https://doi.org/10.1007/s11663-021-02210-w>

© The Minerals, Metals & Materials Society and ASM International 2021

## I. INTRODUCTION

STEEL slags are byproducts of the steelmaking process and are annually generated in vast quantities worldwide. The production of steel slag in Europe was estimated to be approximately 23 million tons in 2018.<sup>[1]</sup> After the liquid slag is separated from the steel, it is cooled, crushed and processed to reclaim valuable and hazardous metals,<sup>[2]</sup> and then the residues can be used as aggregates in road construction,<sup>[3]</sup> additives or raw materials in cement,<sup>[4]</sup> fertilizers in agriculture<sup>[5]</sup> and CO<sub>2</sub> mineralized products.<sup>[6]</sup> Steering of the slag cooling is an effective method to tailor the cold slag's properties for a targeted application and optimize slag valorization.<sup>[7]</sup> In general, the liquid slag is cooled to ambient temperatures, either using water cooling (*i.e.*, a rapid process) or air-cooling (*i.e.*, a slow process). Air-cooled slag, a highly crystalline material, is commonly used as aggregates for road construction, while water-cooled slag, a highly amorphous material, can be used as a binder in the cement industry.<sup>[8]</sup> It is essential to obtain the slag's vital crystallization and temperature information during solidification to manipulate the slag

microstructure for a specific added-value application. The solidified slag's targeted microstructure with designed crystal size, shape, and crystalline to amorphous fraction ratio can be achieved by steering the slag cooling process. However, to date, no online technology has been developed to monitor the slag crystallization behavior in the slag yard of metallurgical plants in order to obtain this information.

The crystallization behavior of slag has been investigated experimentally by various techniques such as quenching experiments and microstructural analysis,<sup>[9]</sup> differential thermal analysis (DTA)<sup>[10]</sup> or differential scanning calorimetry (DSC),<sup>[11]</sup> high-temperature X-ray diffraction (XRD),<sup>[12]</sup> confocal scanning laser microscopy (CSLM),<sup>[13]</sup> and double-hot thermocouple technique (DHTT).<sup>[14]</sup> However, these techniques are either unable to monitor crystallization *in situ* or to quantify its crystallization behavior. The electrical conductivity measurement technique is well developed and is characterized by its low installation and operating cost, efficiency and nondestructive nature. It has been applied to estimate the liquid distribution and fraction in the upper mantle<sup>[15]</sup> and monitor the microstructure evolution in cement-based materials.<sup>[16]</sup> However, there are limited reports on slags' electrical conductivity during solidification except for a few works for molten salts and glasses.<sup>[17,18]</sup> Since the electrical conductivity of materials is sensitive to a minor change in their microstructure, it may be used to monitor the change in the composition of the liquid phase and the solid precipitation during

LING ZHANG, ANNELIES MALFLIET, BART BLANPAIN, and MUXING GUO are with the Department of Materials Engineering, KU Leuven, Kasteelpark Arenberg 44, 3001, Leuven, Belgium. Contact e-mail: ling.zhang@kuleuven.be

Manuscript submitted December 12, 2020; accepted April 29, 2021.

Article published online May 24, 2021.

slag solidification.<sup>[19]</sup> It is crucial to accurately measure the slag electrical conductivity during solidification for this purpose and relate it to the slag microstructure.

A unique experimental setup was developed to measure the electrical conductivity of heterogeneous slags based on the state-of-the-art electrical conductivity measurement technique while simultaneously observing slag solidification in situ. In this way, the slag microstructure correlation with its electrical conductivity can be quantitatively established during the slag solidification process. Two types of high-temperature electrical conductivity cells were developed to understand the influence of the electrode configuration and the crucible material. The reliability of the measurement was confirmed by measuring the electrical conductivity of a standard KCl solution (HI 70031 conductivity solution-1413  $\mu\text{S}/\text{cm}$ , Hanna Instruments, Inc.) at room temperature and a  $\text{CaO-Al}_2\text{O}_3\text{-SiO}_2$  slag at high temperature. The advantages and disadvantages of each cell are evaluated, and recommendations for application are made.

## II. STATE-OF-THE-ART ELECTRICAL CONDUCTIVITY MEASUREMENTS

Electrical conductivity represents a material's ability to conduct an electric charge. It can be calculated from the electrical resistance via the equation:

$$R = \rho \left( \frac{l}{A} \right) = \left( \frac{l}{\sigma} \right) \left( \frac{l}{A} \right) = \frac{l^2}{\sigma A} \quad [1]$$

where  $R$  is the electrical resistance,  $\rho$  is the electrical resistivity,  $\sigma$  is the electrical conductivity,  $l$  is the length of the current path,  $A$  is the cross-sectional area of the current path, and  $G$  is the cell constant. According to Eq. [1],  $G$  plays an important role in an accurate measurement of electrical conductivity. For solids, the

area and length are well defined, and the current path can be determined from the solid's geometry. For liquid, since the current path is not well defined, it is difficult to obtain an accurate cell constant. Therefore, calibration by a standard liquid is usually needed. Calibration can be accomplished by measuring the resistance  $R_{\text{std}}$  of a standard liquid and calculating the cell constant  $G$  by equation.<sup>[1]</sup> The electrical conductivity of the liquid of interest,  $\sigma_{\text{liq}}$ , is then determined by measuring its resistance  $R_{\text{liq}}$  and using the calculated cell constant by the following equation:

$$\sigma_{\text{liq}} = \frac{G}{R_{\text{liq}}} \quad [2]$$

The measurement is valid only when the current path is invariant. Due to different electrical properties between the standard and the liquid of interest, the current path is changed. The most widely used experimental setup for the electrical conductivity measurement of liquid at high temperature involves immersing electrodes with different configurations into a molten bath, applying a voltage, and measuring its resistance. The common electrode setups are depicted schematically in Figure 1. These include crucible, ring, two-wire and four-wire techniques.<sup>[20]</sup> The crucible technique (Figure 1(a)) involves a central rod immersed by a certain depth in the crucible used as another electrode.<sup>[21]</sup> This technique's advantage is that it has a large surface area, which is required for measuring highly conductive materials.<sup>[22]</sup> In the ring technique (Figure 1(b)), two concentric cylinders are used as electrodes, so the current path is well defined between the cylindrical electrodes.<sup>[23]</sup> However, there are still some fringe currents above and below the gap between the electrodes, which cannot be confined. The two-wire method (Figure 1(c)) uses two parallel wires or plates as electrodes.<sup>[24]</sup> The four-wire technique applies a current between two outer electrodes and measures the voltage

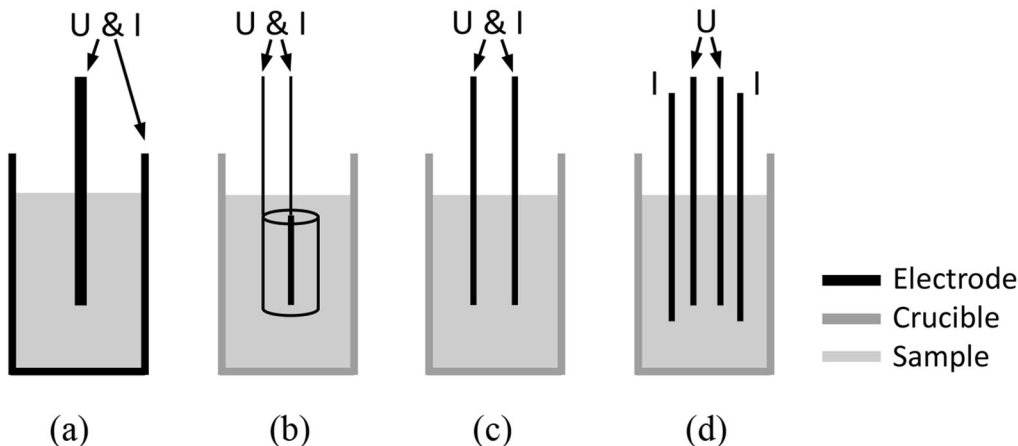


Fig. 1—Electrode configurations typically used in conductivity measurements of liquid: (a) crucible, (b) ring, (c) two-wire, and (d) four-wire.

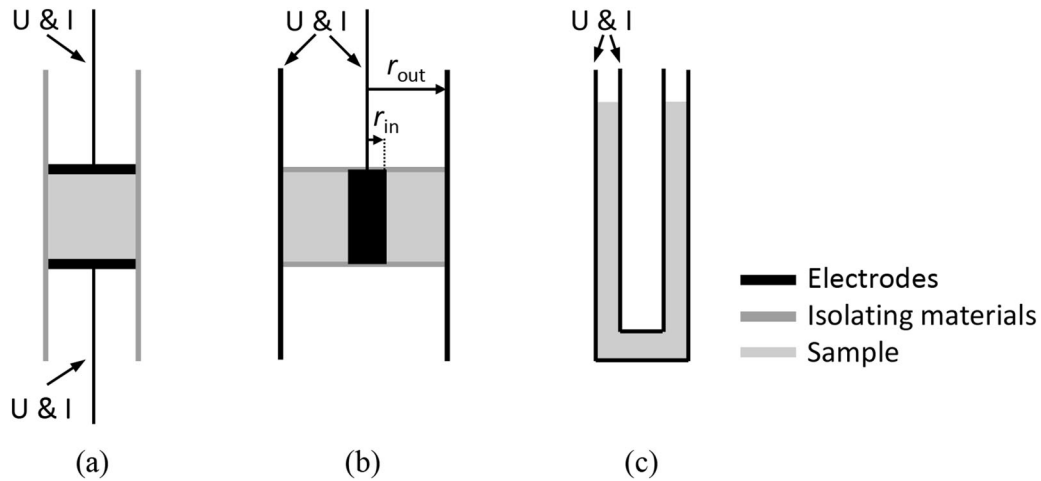


Fig. 2—Experimental setups used in conductivity measurements of pure solid or solid-liquid coexistence systems: (a) two-foil, (b) central, and (c) coaxial cylinders.

between two inner electrodes to avoid interfacial resistance.<sup>[25,26]</sup> However, since the current path cannot be determined for these techniques, calibration is necessary to obtain the cell constant  $G$ .

During the last several decades, new experimental setups have been developed to measure the electrical conductivity of pure solid and solid-liquid systems. Typical setups can be seen in Figure 2 using the two-foil, central electrode and coaxial cylinder arrangements. Since the current path can be directly determined from the geometrical information, they are calibration-free techniques. The two-foil technique (Figure 2(a)) uses two foils as electrodes, and the sample is encapsulated in a ceramic crucible sleeve.  $G$  can be obtained by  $G = l/A$ , where  $A$  is the electrode's surface area, and  $l$  is the sample thickness.<sup>[27]</sup> The central technique (Figure 2(b)) uses a central rod and an outer cylinder as electrodes, and alumina ceramics isolates the sample.<sup>[28]</sup> In this case, the cell constant  $G$  can be calculated from:

$$G = \frac{\ln(r_{out}/r_{in})}{2\pi h} \quad [3]$$

where  $r_{out}$  and  $r_{in}$  are the outer and inner radii of the sample, respectively, and  $h$  is the sample's height. In the coaxial cylinder technique (Figure 2(c)), the sample is placed between two metallic coaxial cylindrical electrodes. The cell constant can be determined using Eq. [3], where  $r_{out}$  and  $r_{in}$  are the radii of the outer and inner cylinders, respectively, and  $h$  is the height of the cylinder. Since the inner electrode has a shorter length than the outer electrode, there is an additional surface at its closed end. Maumus *et al.* introduced a correction factor of ~25 pct into the final calculation of the cell constant to consider this additional surface.<sup>[29]</sup> Although calibration-free techniques might provide more accurate results by eliminating potential calibration errors, the sample geometries and electrodes need to be measured accurately.

### III. DEVELOPMENT OF THE EXPERIMENTAL SETUP MEASURING THE ELECTRICAL CONDUCTIVITY OF HETEROGENEOUS SLAGS WHILE OBSERVING SLAG SOLIDIFICATION IN SITU

#### A. Starting Materials

A synthetic slag was prepared by mixing reagent grade chemicals (*i.e.*, CaO, Al<sub>2</sub>O<sub>3</sub>, SiO<sub>2</sub> powders) and then melting the mixture within a platinum crucible at 1600 °C in air for 2 h in a bottom loading furnace (BLF, AGNI-ELT 160-02 Spring type). The fully melted slag was poured onto a steel plate to obtain a premelted slag. Table I shows the slag's chemical composition, which was determined by an electron probe microanalyser (EPMA) with wavelength dispersive spectroscopy (WDS). As expected, the premelted slag's chemical compositions are the same as that of the powder mixture. The slag liquidus and solidus shown in Table I are calculated using FactSage 7.3 with the FToxid database.

#### B. Experimental Setup and Slag Conductivity Measurement

In the present study, a special setup was developed in the CSLM equipment, which enables the measurement of the slag's electrical conductivity during the in situ CSLM observation of the sample (Figure 3). The electrical conductivity cell assembly was inserted at the upper focal point of the CSLM chamber (the hot zone) and placed on a Pt sample holder equipped with a B-type thermocouple (PtRh). This thermocouple was applied for temperature control of the conductivity cell assembly. A detailed description of the CSLM technique has been reported in previous papers.<sup>[30,31]</sup> In this work, two types of electrical conductivity cells (see the detailed

**Table I. Chemical Composition (Wt Pct) of the Slag as Determined With EPMA-WDS**

	CaO	SiO <sub>2</sub>	Al <sub>2</sub> O <sub>3</sub>	Liquidus (°C)	Solidus (°C)
Powder mixtures	35	55	10	1398	1184
Pre-melted slag	34.76 ± 0.16	55.10 ± 0.34	10.12 ± 0.04	1395	1184

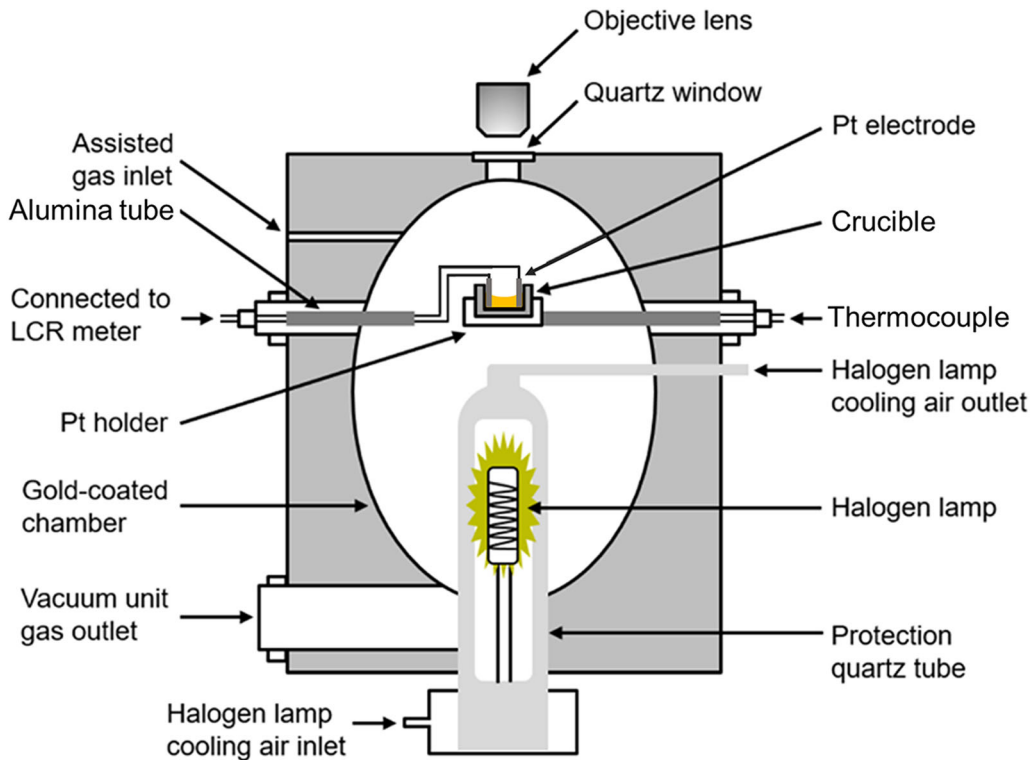


Fig. 3—Schematic diagram of the CSLM.

description in Sect. III.D) were developed for accurate and reliable measurement of the slag's electrical conductivity. In the setup, an LCR (Inductance (L), Capacitance (C), and Resistance (R)) metre (E4980AL Precision LCR Metre, Keysight Co.) was connected through conductive wires to the electrodes of the cell assembly in the CSLM chamber. Temperature calibration was performed using standard pure nickel before the measurement. Figure 4 presents the heating history of the measurement. Before heating, the CSLM chamber was evacuated and flushed with ultrapure argon three times and then flushed continuously with ultrapure argon during the experiments. The synthesized slag sample with the composition shown in Table I was melted at 1500 °C for 3 min to homogenize the chemical composition. Then, electrical conductivity measurements were carried out at 20 to 50 °C intervals during cooling from 1500 °C. Electrical conductivity measurements were conducted using impedance spectroscopy with an LCR metre. Simultaneously, slag behaviour (e.g., solid precipitation) was observed in situ at high temperatures using the CSLM. The melt was kept at each temperature for 3 min to ensure thermal

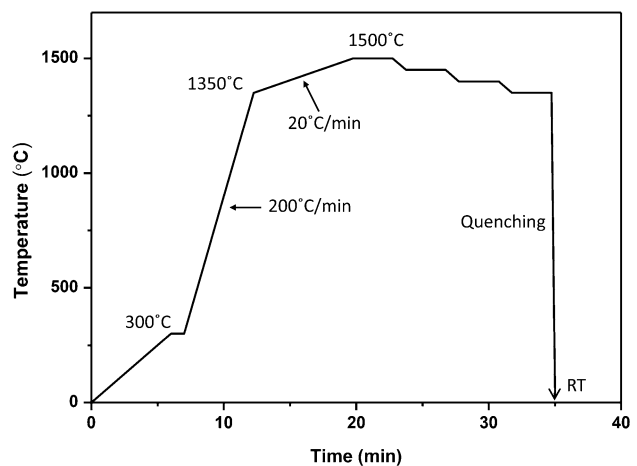


Fig. 4—Temperature profile for electrical conductivity measurement.

equilibrium within the slag. The temperature profiles were controlled by HiTOS software combined with a REX-P300 controller. At the end of the experiments, the

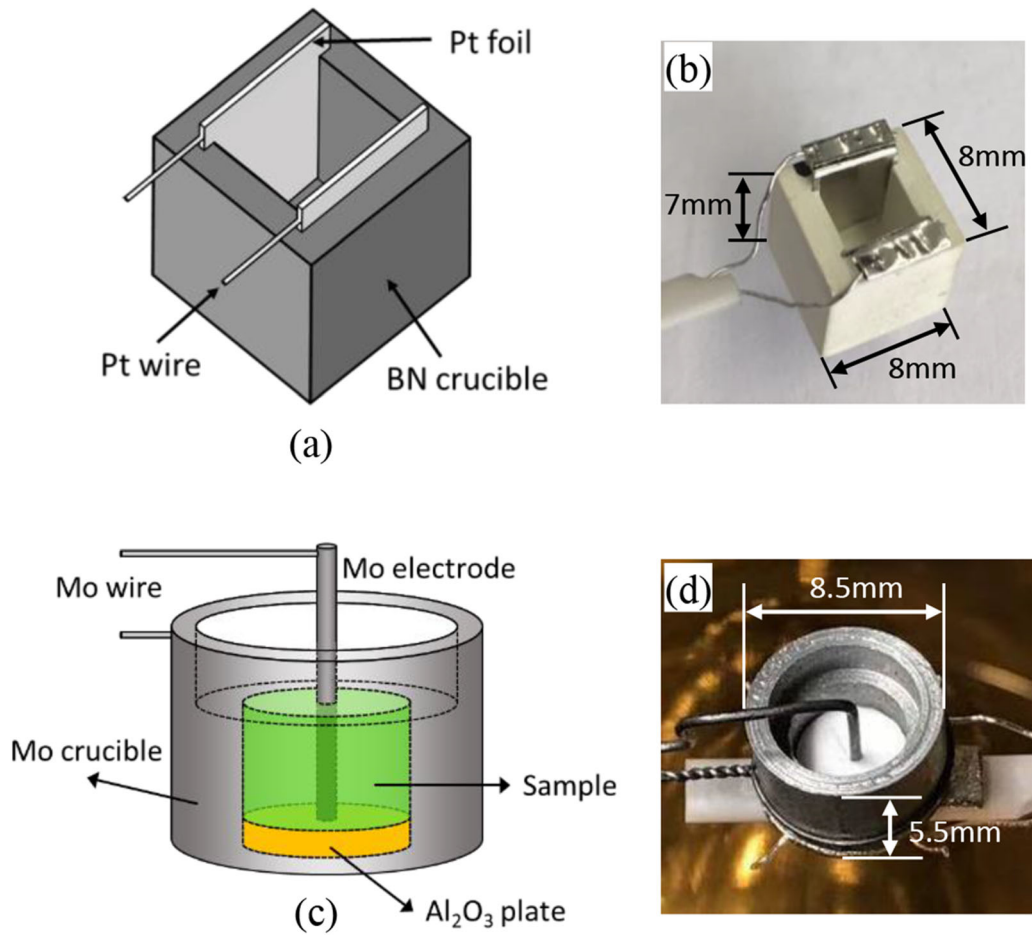


Fig. 5—The two electrical conductivity cell assemblies: (a) 2-electrode cell in BN crucible; (b) photo of the BN crucible cell assembly; (c) 2-electrode cell in Mo crucible; (d) photo of Mo crucible cell assembly.

sample was quenched by shutting off the infrared image furnace's electrical power (IIF) of the CSLM. The quenching temperatures of the BN and Mo crucible cell are 1340 °C and 1350 °C, respectively.

### C. Characterization of the Slag Samples

After the electrical conductivity measurements, the slag samples were mounted in epoxy resin, ground by silicon carbide papers and polished with diamond paste for microstructure analysis. The sample's microstructure was observed with a scanning electron microscope (SEM, FEI XL-40 LaB6). The initial slag's chemical composition and the slag after conductivity measurements were analysed by EPMA (JXA-8530F, JEOL Ltd, Japan) equipped with WDS. The interactions between the conductivity cells (*i.e.*, the crucible, electrode or other cell parts) and the slag were evaluated by SEM and EPMA analysis.

### D. Electrical Conductivity Cell and Determination of Cell Constant

#### 1. Electrical Conductivity Cell

We designed two electrical conductivity cell assemblies to measure the slag's electrical conductivity (Figure 5). For the first cell (Figures 5(a) and (b)), two parallel platinum foils serve as electrodes inside a cubical BN crucible. Boron nitride is used as a crucible material since it is electrically insulating at high temperatures and can be easily machined to a cubical shape, convenient to determine the cell constant (*i.e.*,  $G$  in Eq. [1]). Figures 5(c) and (d) shows the second cell assembly, where a molybdenum wire is inserted into the molybdenum crucible along its axial line and used as the central electrode. Meanwhile, the crucible serves as the other electrode. In this case, the conductivity is measured radially with the 2-electrode method. An alumina plate that electrically isolates the central electrode from



the crucible is placed on the crucible's bottom. An inner step with a smaller inner diameter of the lower part of the crucible is made in the molybdenum crucible to keep the liquid surface at a certain height. Before the conductivity measurement, a small amount of slag was melted in the Mo crucible several times until the liquid level was consistent with the inner step, which can be observed via CSLM. When the liquid level and internal steps are both clear, they are at the same height.<sup>[32]</sup> If there is no inner step, the shape of the sample surface becomes complicated, making it difficult to calculate the cell constant. The second electrical conductivity cell with a Mo crucible is designed to avoid reactions between the slag and BN crucible, resulting in the first cell assembly.

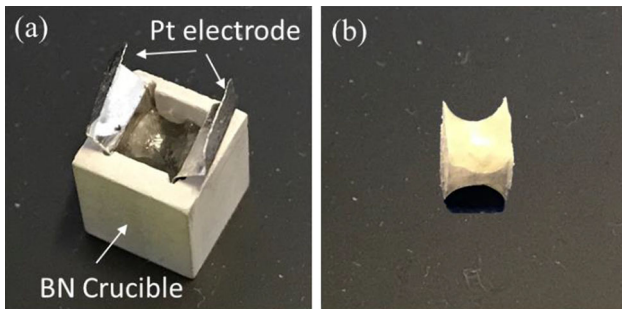


Fig. 6—(a) BN crucible cell containing slag sample after the conductivity measurement; (b) slag sample removed from the BN crucible.

## 2. Determination of the Cell Constant

According to Eq. [1], the determination of the cell constant  $G$  is required to obtain the conductivity  $\sigma$  of the slag through the cell's measured electrical resistance. For the cell with the cubical BN crucible (Figure 5(a)),  $G$  can be calculated by dividing the distance between the two electrodes  $l$  by the cross-sectional area of the current path  $A$ . Since the two Pt plates are fixed in the crucible,  $l$  is a known parameter that is 3.5 mm. The cross-sectional area of the current path  $A$  is determined through the geometry of the slag sample. The latter is obtained by removing the slag sample from the BN crucible or cutting the BN crucible along the plane parallel to the Pt foils after the conductivity measurement. After removing the slag sample from the BN crucible, as shown in Figure 6, the slag sample is not a perfect cube, causing errors when measuring the cross-sectional area. Since the thermal expansion of the  $\text{CaO-Al}_2\text{O}_3\text{-SiO}_2$  slag is estimated to be less than 5 pct from 25 to 1500 °C based on density measurements, it should not significantly affect the cell geometry and is not considered in this study.<sup>[33,34]</sup> For the cell with a cylindrical Mo crucible, the slag sample together with the Mo crucible is cut along an axial plane of the central electrode to obtain the cross-sectional area of the current path  $A$  (Figure 7). The cross-section of the sample is then subjected to SEM observation, and its geometry is measured based on SEM images, as shown in Figure 7(b). In this cell, the charges go through the sample radially from the inner (central) electrode to the outer electrode (Mo crucible). If the sample is divided into concentric cylindrical shells with infinitesimal thickness  $dr$  (Figure 7(a)), all the

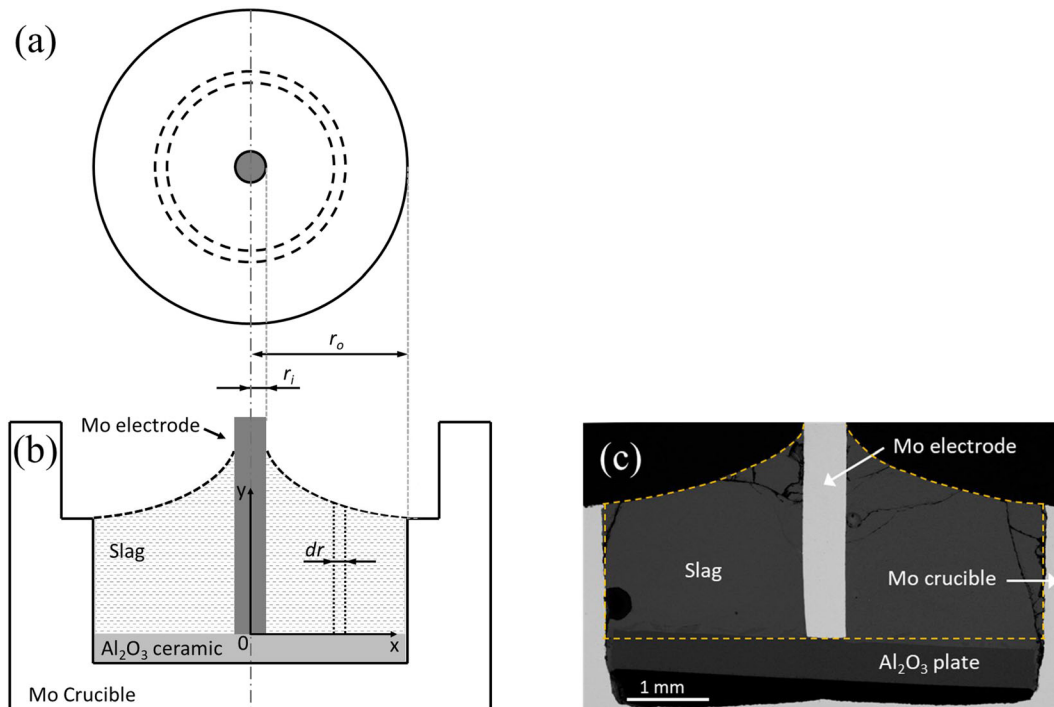


Fig. 7—The molybdenum measurement cell: (a) schematic top view and (b) schematic cross-section of the conductivity cell; (c) cross-section (obtained via SEM) of the quenched sample.

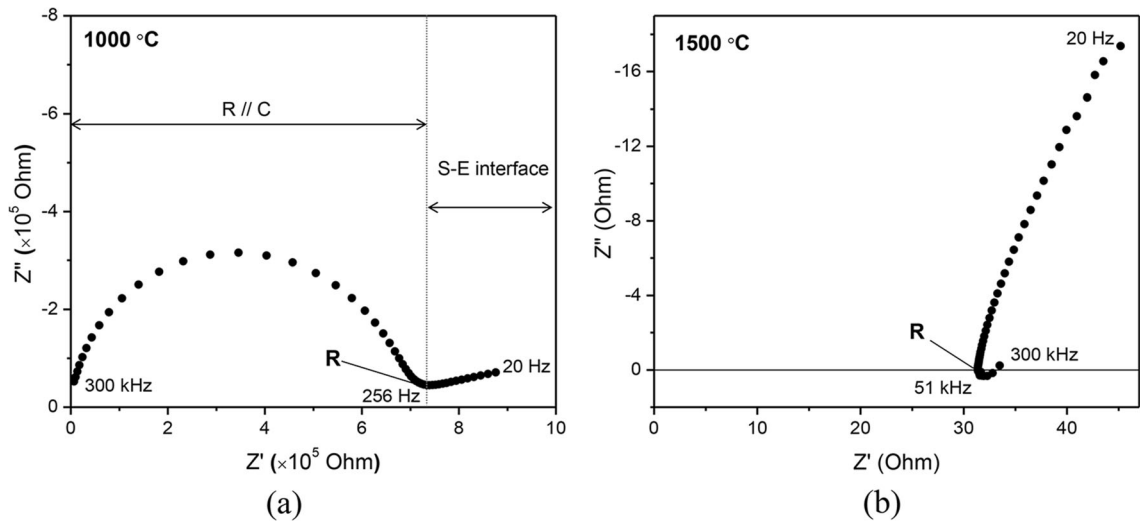


Fig. 8—Electrical response in the Nyquist plane ( $Z'$ ,  $Z''$ ) for slag samples at (a) 1000 °C and (b) 1500 °C.

shells' resistances should be in series. As seen in Figure 7(b), the slag sample's geometry is approximately symmetrical with respect to the axis of the central electrode. Since the height of shell  $h$  can be expressed as a function of the diameter of the cylindrical slag by nonlinear regression ( $h = ar^b$ ), where  $a$  and  $b$  are the fitting parameters, the cell constant  $G$  can be calculated by:

$$G = \int_{r_i}^{r_o} \frac{dr}{2\pi r \cdot ar^b} = \frac{(r_i^{-b} - r_o^{-b})}{2ab\pi} \quad [4]$$

where  $r_i$  and  $r_o$  are the inner and outer radius of the slag sample, respectively.

#### E. Impedance Spectra and Determination of the Resistance of the Slag Sample

Electrical conductivity measurements were conducted using impedance spectroscopy. The electrical conductivity cell was connected to the LCR metre for electrical impedance measurements over the frequency range from 20 Hz to 300 kHz with an applied voltage of 1 V. The measured complex impedance  $Z$  can be expressed by  $Z = Z' + jZ''$  (with  $j = \sqrt{-1}$ ), where the imaginary part  $Z''$  results from the capacitance or inductance of a dielectric material. The real part corresponds to the sample's electrical resistance  $R$ , from which the corresponding electrical conductivity value of the sample is obtained by using Eq. [2]. The frequency-dependent electrical response of the sample can be directly depicted in the Nyquist plane, where the shape of the impedance spectra (*i.e.*, shape of the  $Z'$ ,  $Z''$  relation curve), in general, is arc-like at high frequency with an additional tail at low frequency, as shown in Figure 8(a). The arc at high frequency represents the sample's electrical response, and the tail at low frequency reflects the effect

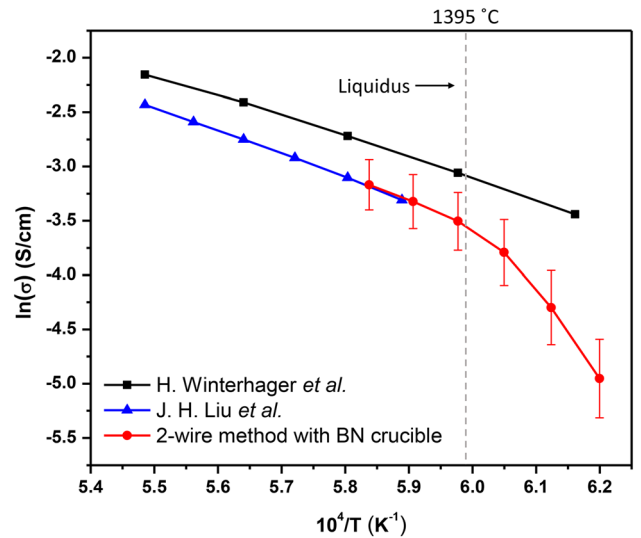


Fig. 9—The measured conductivity of the 35 wt pct CaO-10 wt pct  $\text{Al}_2\text{O}_3$ -55 wt pct  $\text{SiO}_2$  slag as a function of temperature using the BN crucible cell (Adapted from Refs. 31, 32).

of the interface between the sample and electrode.<sup>[35]</sup> In this context, the first arc is used to determine the sample resistance, which is the impedance value  $Z'$  at the point closest to the real axis. An arc appears for the test at 1000 °C equivalent to a parallel resistance and capacitance circuit, as shown in Figure 8(a). For the test at 1500 °C, it is difficult to distinguish the arc (Figure 8(b)) because, at 1500 °C, the slag sample is an ionic liquid that exhibits no capacitor response in the high-frequency range. A quasi-linear part in the low-frequency range is observed for this case, and the sample's resistance  $R$  is derived from its intersection with the axis of the real part  $Z'$ .<sup>[36]</sup>

#### IV. RESULTS AND DISCUSSION

The electrical conductivity of a standard KCl solution at room temperature and a CaO-Al<sub>2</sub>O<sub>3</sub>-SiO<sub>2</sub> slag at high temperature was measured to evaluate the measurement cell's accuracy. The KCl solution's conductivity was not measured with the BN crucible cell since the standard KCl solution's surface is not flat in the BN crucible cell. CaO, MgO and Al<sub>2</sub>O<sub>3</sub> are common oxides often found in metallurgical slag, and numerous conductivity data are available, so a composition of CaO-Al<sub>2</sub>O<sub>3</sub>-SiO<sub>2</sub> slag with suitable liquidus was selected to verify the measurement at high temperature. After the measurements, the advantages and disadvantages of each cell are compared and evaluated.

##### A. Electrical Conductivity Measured Using the BN Crucible Cell

Figure 9 shows the natural logarithm of the electrical conductivity measured using the 2-electrode cell in the BN crucible as a function of the reciprocal temperature for the 35 wt pct CaO-10 wt pct Al<sub>2</sub>O<sub>3</sub>-55 wt pct SiO<sub>2</sub> slag, which is compared with the electrical conductivity data of the same slag measured by Winterhager *et al.*<sup>[37]</sup> and Liu *et al.*<sup>[38]</sup> In general, the electrical conductivity of a material represents the ability to conduct electric current, which is proportional to the product of mobility and carrier concentration. It has been widely accepted that the temperature dependence of electrical conductivity can be expressed by the Arrhenius relationship<sup>[39]</sup>:

$$\sigma = \sigma_0 \exp(-E_a/RT) \quad [5]$$

where  $\sigma$  is the electrical conductivity (S/cm);  $\sigma_0$  is the pre-exponential factor;  $E_a$  is the activation energy (J·mol<sup>-1</sup>·K<sup>-1</sup>); R is the gas constant (8.314 J·mol<sup>-1</sup>·K<sup>-1</sup>); T is the absolute temperature (K). As seen in Figure 9, when the temperature is higher than the slag liquidus, the logarithm of the slag's electrical conductivity linearly decreases with the reciprocal of the temperature for both the current measurement and

the results of Winterhager *et al.*<sup>[37]</sup> and Liu *et al.*,<sup>[38]</sup> implying that the temperature dependence of the slag conductivity follows the Arrhenius law.

Below the liquidus temperature, unlike the results of Winterhager *et al.*,<sup>[37]</sup> this linear relationship does not hold, suggesting heterogeneous slag with solid precipitation. Under the same conditions as Winterhager *et al.*,<sup>[37]</sup> due to the different crucible materials, solid precipitates were formed. This is confirmed by the in situ CSLM observation of the slag solidification behaviour when measuring the slag's electrical conductivity. As seen in Figure 10, solid precipitates are observed at 1380 °C, below the slag's liquidus temperature. The presence of solid particles in the liquid slag decreases the number of charge carriers, resulting in a sharper slope of the  $\ln(\sigma) \cdot 10^4/T$  relationship for the slag conductivity. The increasing difference in slag electrical conductivity between the current measurement and the results of Winterhager *et al.*<sup>[37]</sup> with decreasing temperature suggests that a more considerable amount of crystals precipitated during cooling in the present experiment. By combining the results of the in situ observation of solid precipitation with the measured electrical conductivity data, a quantitative electrical conductivity-solid fraction relationship can therefore be identified using this 2-electrode BN crucible cell.

In the temperature region above the slag liquidus, the present conductive data are very close to the results of Liu *et al.*<sup>[38]</sup> but systematically lower than the results of Winterhager *et al.*<sup>[37]</sup> (see Figure 9). This difference is probably due to the use of the ring electrode technique (see Figure 1 (b)) at a fixed frequency of 50 kHz in the measurement of Winterhager *et al.*,<sup>[37]</sup> where calibration in a standard solution is required for the determination of the cell constant, causing an extra error when the standard and sample are not measured under precisely the same conditions. Liu *et al.*<sup>[38]</sup> used the four-wire technique (see Figure 1 (d)) at a fixed frequency of 20 kHz, which also requires calibration but can eliminate interfacial resistance. Moreover, their experimental data

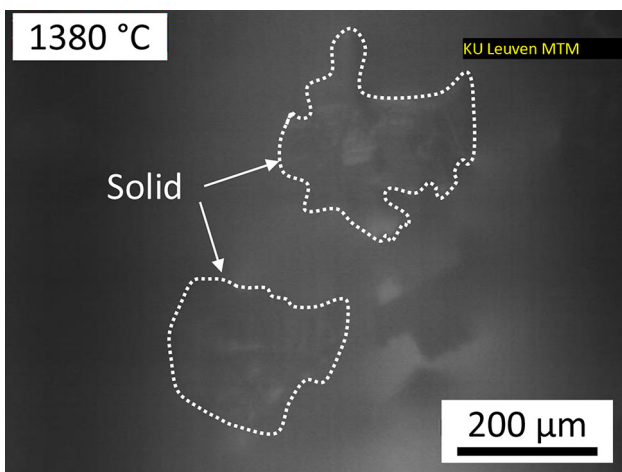


Fig. 10—Illustration of solid precipitation in the CSLM test with the 35 wt pct CaO-10 wt pct Al<sub>2</sub>O<sub>3</sub>-55 wt pct SiO<sub>2</sub> slag using the BN crucible cell.

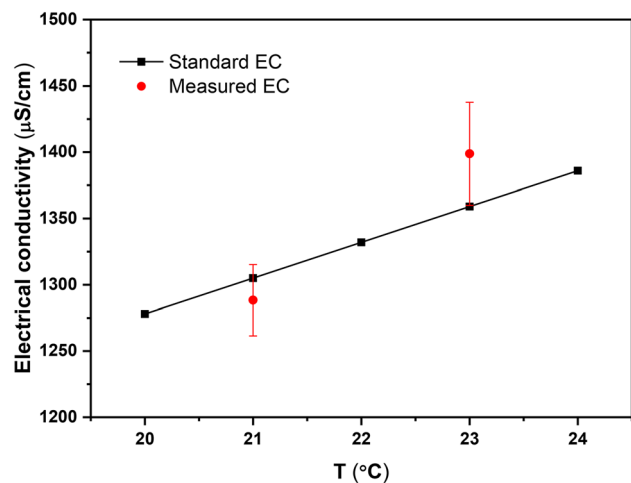


Fig. 11—The standard KCl solution's measured conductivity as a function of temperature using the Mo crucible cell.



is more recent. The accuracy of the experimental results is strongly influenced by the electrode configuration, required calibration, and by the electric circuit design, frequency range, crucible, and electrode materials.<sup>[40]</sup> The current conductivity measurement is a calibration-free technique that provides more accurate results by removing the potential errors in calibration. The main error in this technique comes from the geometric measurement of the slag sample used for cell constant determination. A Mo crucible cell is developed, and the measurement results are discussed in section 4.2 to avoid possible reactions between the slag and the BN crucible for some slag systems.

### B. Electrical Conductivity Measured Using a Mo Crucible Cell

The current Mo crucible cell (Figure 5(b)) aims to measure the slag's electrical conductivity that may react with the BN crucible. Before the high-temperature experiments, this Mo crucible cell was applied to measure the standard KCl solution's electrical conductivity with known electrical conductivity to validate the cell at room temperature. The measurement was repeated three times at 21 °C and 23 °C, and the results are shown in Figure 11. Moreover, the measurement fluctuation is indicated by the error bars, and the known electrical conductivity of the standard solution is also plotted for comparison. The current result is in good agreement with the standard conductivity value. The mean absolute percentage deviation (MAPD) is used to evaluate the accuracy of the present work. Specifically,

$$\Delta = \frac{1}{N} \times \sum_{i=1}^N \frac{|\sigma_m - \sigma_s|}{\sigma_s} \times 100\text{pct} \quad [6]$$

where  $\sigma_m$  and  $\sigma_s$  are the measured conductivity, and standard conductivity, respectively, and N represents the number of measurements. The MAPD ( $\Delta$ ) between the measured data and the standard value is only 2.4 pct. This further confirms the reliability of the present Mo crucible setup for the measurement at room temperature.

Figure 12 shows the natural logarithm of the electrical conductivity measured using the 2-electrode cell in a Mo crucible as a function of the reciprocal temperature for the 35 wt pct CaO-10 wt pct Al<sub>2</sub>O<sub>3</sub>-55 wt pct SiO<sub>2</sub> slag, which is also compared with the electrical conductivity data of the slag measured by Winterhager *et al.*<sup>[37]</sup> and Liu *et al.*<sup>[38]</sup> Unlike the BN crucible cell (Figure 9), the slag conductivity's temperature dependence follows the Arrhenius law in the temperature range both above and below the slag liquidus, meaning the slag was still fully liquid even though it was cooled below the liquidus; consistent with the *in situ* CSLM observation, as shown in Figure 13, where no solid precipitation was observed during the measurement below the liquidus. This is probably attributed to (1) the inner wall of the Mo crucible is smoother than that of the BN crucible, which is not conducive to heterogeneous nucleation; (2) the Mo crucible has a higher thermal conductivity than

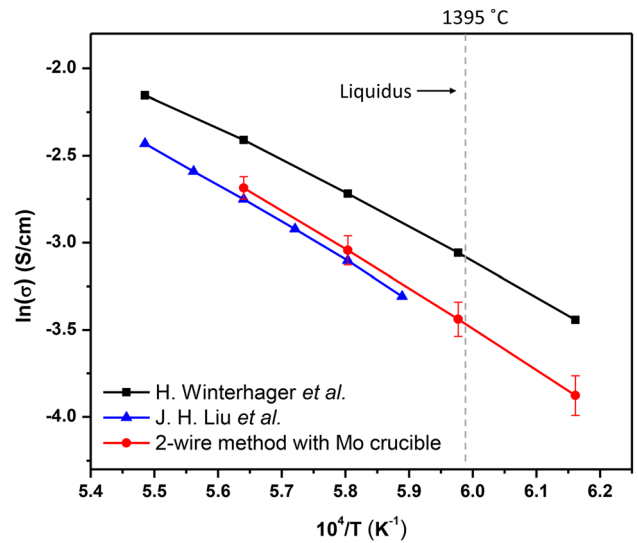


Fig. 12—The measured conductivity of the 35 wt pct CaO-10 wt pct Al<sub>2</sub>O<sub>3</sub>-55 wt pct SiO<sub>2</sub> slag as a function of temperature using the Mo crucible cell (Adapted from Refs. <sup>[31, 32]</sup>).

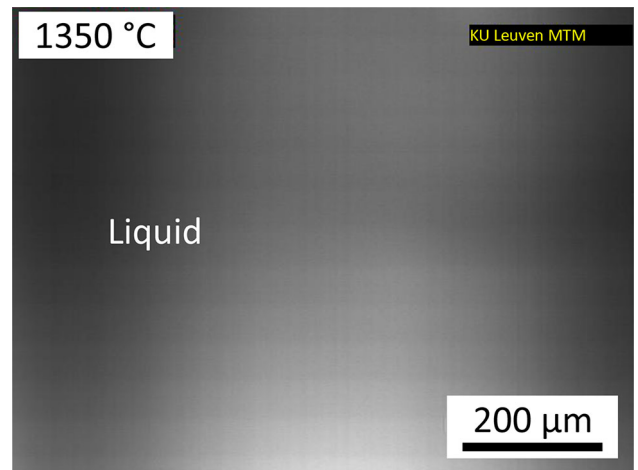


Fig. 13—Illustration of liquid slag in the CSLM test with the 35 wt pct CaO-10 wt pct Al<sub>2</sub>O<sub>3</sub>-55 wt pct SiO<sub>2</sub> slag using the Mo crucible cell.

the BN crucible, which results in a faster cooling of the slag in the Mo crucible cell and therefore insufficient time for nucleation and growth of the solid phase. The measurement was repeated three times at each temperature, and the MAPD was estimated by Equation <sup>[6]</sup> to be approximately 6 pct, while for the BN cell, it was approximately 11 pct. The relatively higher deviation for the BN cell is mainly attributed to the low wettability of molten slag in the BN crucible. Therefore, a perfect cubic geometry of the slag sample could not be obtained, leading to an error in the cell constant determination (see Figure 6(b)). In the case of the Mo cell, the cell constant can be precisely determined by using the well-established sample geometry after the measurement (see Figure 7). In addition, the Mo cell can

be applied to the slag system that chemically reacts with BN crucible cells but not to highly oxidizing slags, such as FeO/Fe<sub>2</sub>O<sub>3</sub> and MnO.

## V. CONCLUSIONS

In this work, a unique experimental setup was developed using a confocal scanning laser microscope (CSLM) to measure the electrical conductivity of metallurgical slags while simultaneously observing the slag solidification behaviour *in situ* during cooling. Two types of electrical conductivity cells were developed to determine the electrical conductivity of the slag. The technique's accuracy was evaluated by measuring the electrical conductivity of a standard conductivity solution and the molten slag and comparing these data with their reference values. The main conclusions are:

- (1) By combining the results of the *in situ* observation of the slag microstructure with the measured electrical conductivity data, the relationship of the electrical conductivity and slag microstructure can be determined using the developed 2-electrode BN crucible cell and Mo crucible cell.
- (2) The BN crucible cell can be applied to measure the electrical conductivity of slags that do not react with boron nitride, while the Mo crucible cell can be applied to measure slags that chemically react with the BN crucible but not to measure highly oxidizing slags. The appropriate electrical conductivity cell can be selected for the measurement depending on the application conditions.
- (3) The developed techniques are confirmed to be reasonably accurate and reliable for the *in situ* observation of slag solidification and the simultaneous measurement of the slag's electrical conductivity.

## ACKNOWLEDGMENTS

Ling Zhang acknowledges the support of the KU Leuven Hitemp Centre and the China Scholarship Council (CSC).

## REFERENCES

1. Steel slag production data, [www.euroslag.com](http://www.euroslag.com). Accessed 1 May 2020.
2. H. Shen and E. Forssberg: *Waste Manag.*, 2003, vol. 23, pp. 933–49.
3. Y. Xue, S. Wu, H. Hou, and J. Zha: *J. Hazard. Mater.*, 2006, vol. 138, pp. 261–68.
4. S.Z. Carvalho, F. Vernilli, B. Almeida, M. Demarco, and S.N. Silva: *Resour. Conserv. Recycl.*, 2017, vol. 127, pp. 216–20.
5. X. Wang and Q.-S. Cai: *Pedosphere*, 2006, vol. 16, pp. 519–24.
6. S.Y. Pan, R. Adhikari, Y.H. Chen, P. Li, and P.C. Chiang: *J. Clean. Prod.*, 2016, vol. 137, pp. 617–31.

7. D. Durinck, F. Engström, S. Arnout, J. Heulens, P.T. Jones, B. Björkman, B. Blanpain, and P. Wollants: *Resour. Conserv. Recycl.*, 2008, vol. 52, pp. 1121–31.
8. C. Shi: *J. Mater. Civ. Eng.*, 2004, vol. 16, pp. 230–36.
9. Z. Liu, L. Chen, B. Blanpain, and M. Guo: *ISIJ Int.*, 2018, vol. 58, pp. 1972–78.
10. J. Li, Q. Shu, and K. Chou: *Metall. Mater. Trans. B*, 2015, vol. 46B, pp. 1555–63.
11. M.-D. Seo, C.-B. Shi, J.-W. Cho, and S.-H. Kim: *Metall. Mater. Trans. B*, 2014, vol. 45B, pp. 1874–86.
12. M. Suzuki, H. Serizawa, and N. Umesaki: *ISIJ Int.*, 2020, vol. 60, pp. 2765–72.
13. I. Sohn and R. Dippenaar: *Metall. Mater. Trans. B*, 2016, vol. 47, pp. 2083–94.
14. J. Yang, J. Zhang, Y. Sasaki, O. Ostrovski, C. Zhang, D. Cai, and Y. Kashiwaya: *Metall. Mater. Trans. B*, 2016, vol. 47B, pp. 2447–58.
15. T. Yoshino, M. Laumonier, E. McIsaac, and T. Katsura: *Earth Planet. Sci. Lett.*, 2010, vol. 295, pp. 593–602.
16. K.B. Sanish, N. Neithalath, and M. Santhanam: *Constr. Build. Mater.*, 2013, vol. 49, pp. 288–97.
17. S. Pietrzyk and R. Oblakowski: in *Light metals-Warrendale-Proceedings*, TMS, 2002, pp. 231–38.
18. C. Simonnet, J. Phalippou, M. Malki, and A. Grandjean: *Rev. Sci. Instrum.*, 2003, vol. 74, pp. 2805–10.
19. L. Zhang, A. Malfiet, B. Blanpain, and M. Guo: in *6th International Slag Valorisation Symposium*, Mechelen, 2019, pp. 137–40.
20. S.L. Schiefelbein, N.A. Fried, K.G. Rhoads, and D.R. Sadoway: *Rev. Sci. Instrum.*, 1998, vol. 69, pp. 3308–13.
21. R.A. Berryman: Ph.D. Thesis, University of Toronto, Toronto, 1989.
22. H. Inouye, J.W. Tomlinson, and J. Chipman: *Trans. Faraday Soc.*, 1953, vol. 49, pp. 796–801.
23. M. Kawahara, Y. Ozima, K. Morinaga, and T. Yanagase: *J. Jpn. Inst. Met.*, 1974, vol. 42, pp. 618–23.
24. C. Sun and X. Guo: *Trans. Nonferrous Met. Soc. China*, 2011, vol. 21, pp. 1648–54.
25. S. Hara, H. Hashimoto, and K. Ogino: *Trans. Iron Steel Inst. Japan*, 1983, vol. 23, pp. 1053–8.
26. M. Barati and K.S. Coley: *Metall. Mater. Trans. B*, 2006, vol. 37, pp. 41–9.
27. A. Pommier, K. Leinenweber, and M. Tasaka: *Earth Planet. Sci. Lett.*, 2015, vol. 425, pp. 242–55.
28. A. Pommier, F. Gaillard, M. Pichavant, and B. Scaillet: *J. Geophys. Res. Solid Earth*, 2008, vol. 113, pp. 1–16.
29. J. Maumus, N. Bagdassarov, and H. Schmeling: *Geochim. Cosmochim. Acta*, 2005, vol. 69, pp. 4703–18.
30. J.J. Liu, G. Chen, P.C. Yan, B. Blanpain, N. Moelans, and M. Guo: *J. Cryst. Growth*, 2014, vol. 402, pp. 1–8.
31. J. Liu, M. Guo, P.T. Jones, F. Verhaeghe, B. Blanpain, and P. Wollants: *J. Eur. Ceram. Soc.*, 2007, vol. 27, pp. 1961–72.
32. H. Chikama, H. Shibata, T. Emi, and M. Suzuki: *Mater. Trans. JIM*, 1996, vol. 37, pp. 620–26.
33. L.R. Barrett and A.G. Thomas: *J. Soc. Glas. Technol.*, 1959, vol. 43, pp. 179–90.
34. L. Muhmood and S. Seetharaman: *Metall. Mater. Trans. B*, 2010, vol. 41B, pp. 833–40.
35. J.J. Roberts and J.A. Tyburczy: *Surv. Geophys.*, 1994, vol. 15, pp. 239–62.
36. J.S. Huebner and R.G. Dillenburg: *Am. Mineral.*, 1995, vol. 80, pp. 46–64.
37. H. Winterhager, L. Greiner, and R. Kammel: in *Westdeutscher Verlag*, Cologne, 1966, pp. 14, 23–24.
38. J.-H. Liu, G.-H. Zhang, and K.-C. Chou: *Can. Metall. Q.*, 2015, vol. 54, pp. 170–76.
39. Q. Jiao and N.J. Themelis: *Metall. Trans. B*, 1988, vol. 19, pp. 133–40.
40. E. Thibodeau and I.-H. Jung: *Metall. Mater. Trans. B*, 2016, vol. 47B, pp. 355–83.

**Publisher's Note** Springer Nature remains neutral with regard to jurisdictional claims in published maps and institutional affiliations.